Self-deicing Electrolyte Hydrogel Surfaces with Pa-level Ice Adhesion and Durable Anti-freezing/frost Performance

Journal:	*ACS Applied Materials & Interfaces*
Manuscript ID	am-2020-069127.R2
Manuscript Type:	Article
Date Submitted by the Author:	07-Jul-2020
Complete List of Authors:	Li, Tong; Norwegian University of Science and Technology, Dept. of Structural Engineering Ibáñez Ibáñez, Pablo F.; Norwegian University of Science and Technology, Dept. of Structural Engineering; Universidad de Granada, Department of Applied Physics Håkonsen, Verner ; Norges teknisk-naturvitenskapelige universitet Wu, Jianyang; Norwegian University of Science and Technology, Dept. of Structural Engineering; Xiamen University, Department of Physics Xu, Ke; Xiamen University, Department of Physics Zhuo, Yizhi; Norwegian University of Science and Technology, Department of Structural Engineering Luo, Sihai; NTNU, Chemistry He, Jianying; Norges teknisk-naturvitenskapelige universitet Zhang, Zhiliang; Norges teknisk-naturvitenskapelige universitet,

Self-deicing Electrolyte Hydrogel Surfaces with Pa-level Ice Adhesion and Durable Anti-freezing/frost Performance

Tong Li[a], Pablo F. Ibáñez-Ibáñez[a,b], Verner Håkonsen[a], Jianyang Wu[a,c], Ke Xu[c], Yizhi Zhuo[a], Sihai Luo[d], Jianying He[a*] and Zhiliang Zhang[a*]

[a] NTNU Nanomechanical Lab, Department of Structural Engineering, Norwegian University of Science and Technology (NTNU), 7491, Trondheim Norway.

[b] Laboratory of Surface and Interface Physics (LSIP), Applied Physics Department, Faculty of Sciences, University of Granada, Campus de Fuentenueva s/n, ES 18071 Granada, Spain.

[c] Department of Physics, Research Institute for Biomimetics and Soft Matter, Fujian Provincial Key Laboratory for Soft Functional Materials Research, Xiamen University, Xiamen 361005, PR China.

[d] Department of Chemistry, Norwegian University of Science and Technology (NTNU), 7491, Trondheim, Norway.

[*]E-mail: zhiliang.zhang@ntnu.no, jianying.he@ntnu.no.

Keywords: anti-icing, ice adhesion strength, anti-freezing, anti-frost, durability

Abstract

Despite the remarkable advances in mitigating ice formation and accretion, however, no engineered anti-icing surfaces today can durably prevent frost formation, droplet freezing and ice accretion in an economical and eco-friendly way. Herein, sustainable and low-cost electrolyte hydrogel (EH) surfaces are developed by infusing salted water into the hydrogel matrix for avoiding icing. The EH surfaces can both prevent ice/frost formation for an extremely long time and reduce ice adhesion strength to ultralow value (Pa-level) at a tunable temperature window down to -48.4 °C. Furthermore, ice can self-removes from the tilted EH surface within 10 s at -10 °C by self-gravity. As demonstrated by both molecular dynamics simulations and experiments, these extreme performances are attributed to the diffusion of ions to the interface between EH and ice. The sustainable anti-icing properties of EH can be maintained by replenishing in real-time with available ion sources, indicating the promising applications in offshore platforms and ships.

Introduction

Ice formation and accretion, via frost, snow, and freezing rain, results in severe challenges for infrastructures and transportation, including the collapse of grid infrastructures, failure of turbine blades and traffic accidents.[1-3] These hazards can be divided into two aspects. Firstly, ice formation on surface (e.g. frost, rime) can cause change of the intrinsic surface properties, such as optical property and wettability.[4-5] Secondly, ice accretion on surface can result in a loss of equipment efficiency and even the destruction of infrastructure by the gravity of ice.[6-7] A general anti-icing strategy requires the surfaces to possess effective functionalities, namely to truly prevent ice formation and/or to have low ice adhesion strength for easy removal of eventually formed ice.

The current industrial practices, including mechanical, chemical and thermal deicing methods, despite effectiveness, are energy-intensive and/or environmentally unfriendly.[8] To solve the high cost of deicing associated environmental challenges, various anti-icing or icephobic surfaces have been developed, including superhydrophobic surfaces (SHS),[9-10] interfacial slippage surfaces (ISS),[2, 7, 11] cracks/modulus controlled low ice adhesion surfaces,[8, 12-13] and lubricating surfaces.[14-21] They mitigate the hazards by delaying ice formation time and/or reducing ice adhesion strength on surfaces. However, the delayed ice formation time of these surfaces is limited and/or the reduction of ice adhesion is not significant enough, which has not reached for practical requirements of durable anti-freezing/frost and self-removal of ice.[7, 22] For example, SHS delay ice formation within a limited time by repelling water droplets,[9] and they increase ice adhesion because of interlocking effect.[23-24] The durable low ice adhesion is obtained from extremely soft ISS surfaces, however, their poor mechanical properties restricted the practical applications.[2, 7] Macrocrack initiators (MACI), stress localization and modulus reduction strategies, have been found to reduce the ice adhesion of surfaces by prompting crack initiation and propagation via stiffness inhomogeneity and deformation incompatibility.[8, 12-13, 25-26] However, the ice adhesion strength of these methods are still in the need for reduction for the self-removal of ice. The lubricating surfaces (surfaces with lubricating layer), including slippery lubricant-infused surfaces (SLIS) and hydrated surfaces, mitigate ice formation and reduce ice adhesion.[14, 16, 18, 27-29] However, ice will form on the SLIS, as the depletion of organic lubricant from SLIS results in the reduction of icephobic ability.[27, 30] In contrast, the hydrated surfaces self-generate the aqueous lubricating layer at interface between ice and materials, opening a sustainable avenue to mitigate ice formation and lower ice adhesion. So far, antifreeze proteins, ethanol/water and

polyelectrolytes with counterions have been used to develop the hydrated surfaces to mitigate the ice challenge.[20, 28, 31-33] For example, the ice formation time has been delayed to ca. 4500 s and the ice adhesion has been reduced to ca. 20 kPa on the polyelectrolyte hydrogel surface simultaneously.[21] Nonetheless, the ice could form on the hydrated surfaces after the delay-time and the ice adhesion need further improvement. It remains a daunting challenge to avoid ice formation and accretion.

Herein, we report an easy and low-cost method to truly prevent the ice hazards by employing transparent electrolyte hydrogels (EHs), which are fabricated by infusing salted water into the polymer network. The EH surfaces can durably prevent ice formation and have ultralow ice adhesion simultaneously within a tunable anti-icing temperature range (down to -48.4 ^{o}C). The Molecular dynamics (MD) simulations and in situ experiments show that the diffusion of ions to the interface lead to the melt of ice crystals. In addition, the EH can be quickly replenished with the salted water (e.g. straight forward seawater), resulting in sustainable icephobicity. Our strategy could potentially be used as a sustainable ice protection system in the offshore platforms and ships.

Results and discussion

1 Morphology, composition and properties of EH.

To demonstrate the anti-icing/icephobic properties of EHs, they were fabricated by infusing sodium chloride (NaCl) as a typical ions source into the polyvinyl alcohol (PVA) hydrogel, resulting in a solid compound with liquid inside. The EH sample prepared from 20 wt. % aqueous NaCl solution is used for investigation unless stated otherwise. The fabrication procedure of EH is shown in Figure 1 a and b as well as the experimental part. As shown in Figure 1b, the PVA hydrogel shrinks after soaking in comparison with the EH, due to the loss of water from the hydrogel caused by the concentration difference.[34] Finally, the as-prepared EH was obtained with a thickness of 1.2 mm after further soaking without obvious volume and weight change, indicating that the concentration of ions in PVA hydrogel and NaCl solution reached an equilibrium. As shown in Figure 1b (3), the obtained EH shows a transparent character with an average transmittance of *ca.* 90.0% at the wavelength range of 400-800 nm (Figure S1). Two and three-dimensional atomic force microscopy (AFM) images (Figure 1c,d) reveal that the EH surface is smooth, with a root-mean-square roughness of 5 nm from an area of 500×500 nm^2.

Furthermore, EDS test and weight measurement reveal that the EH consists of 40.7 wt.% water, 30.0 wt.% ions and 29.3 wt.% PVA matrix, demonstrating the ions have been infused into the hydrogel. (Supporting Information, Figure S2 and S3). Furthermore, Raman spectroscopy was performed to reveal the existent configuration of water inside the EH. The peak (symmetric –OH stretch) shifts from about 3410 cm^{-1} to about 3457 cm^{-1} (blue arrow in Figure 1e), and the shoulder peak (3220 cm^{-1}, asymmetric –OH stretch) decreases significantly in comparison to Raman spectra of PVA hydrogel and water, demonstrating that the configuration of water is strongly influenced by ions. This is consistent with previous studies of the influence on the configuration of water by ions (NaCl),[35] in which the ions and water molecules in EH interact with each other and form hydrated ions in comparison with random water molecules (Figure S4b). Furthermore, the crystallization/melting points of EHs with variable concentration of ions (0, 5, 10, 15, 20 and 23 wt. %) are revealed by the differential scanning calorimetry (DSC) tests (Figure S5a shows an example about how to identify the points), with obtained values summarized in Figure 1f; The crystallization/melting points of EHs decrease from -17.3/1.7 ^{o}C to -47.1/-21.8 ^{o}C with the concentration of ions increasing from 0 to 23 wt. %, due to the hydration.[36-37]. The crystallization/melting points of EH are also compared with those of water, 20 wt. % NaCl solution and PVA hydrogel (Figure S5b), revealing that the reduction of crystallization/melting points of EH is due to the addition of NaCl solution. Notably, it is due to the lack of nucleation sites during the cooling process, resulting in much lower crystallization points than the melting points. Hence, the melting point is used to characterize the anti-freezing point of EH.

2 Anti-icing mechanism of EH surface.

According to our hypothesis, the ions inside the EH have mobility. They may diffuse to the interface due to the osmotic pressure between EH and ice/supercooled water, and then interact with the ice or supercooled water (Figure 2a-c). Consequently, ice crystals can be inhibited from formation or broken up, resulting in the generation of liquid lubricating layer at interface (Figure 2c). The mechanism of the destruction of ice crystals by ions at the interface is firstly demonstrated by MD simulations (Supporting Information, Figure S6). The results show that the ice crystal is destroyed by ions, due to electrostatic and van der Waals interaction between the ions and ice crystal. Moreover, detailed information is shown in the Supporting Information to demonstrate the process. Figure 2d shows an image of the pilot process images via the MD simulations of ice and cooled water, in which a part of the ice is destroyed and forms a liquid state. Figure 2e further reveals the melting rate of ice decreases with the decrease of

temperature (from -5 to -15°C), indicating that the generation of the lubricating layer is positively correlated to temperature.

Furthermore, the self-melting of ice at EH surface is demonstrated by in situ observation of a 5 μL ice on the EH surface at -10 °C. As shown in Figure 2f, the morphology of the ice changes from a dark opaque triangular-like appearance (0 s) to a transparent hemispherical shape (2077s), indicating that the ice is melting with time at -10 °C on the EH surface. In detail, the slight transparent part of the droplet, close to the surface, firstly appearing at 70 s, demonstrates the rapid formation of liquid water. As time progresses, the area and transparency of the droplet increase, showing the continued melting of the ice. The melting of ice from the interface to the top of the ice, which is consistent with the MD simulations results that ice melts starting from the interface. Finally, after 2077 s, the ice melts completely. Notably, the ice melts at the interface immediately from MD results; no observed transparency was seen at 0-60 s between the interface in Figure 2f, which is probably due to the resolution and restriction of the current observing method. Furthermore, the melting rate of the droplet can be roughly assessed based on the area of the transparent part of the droplet from 90 to 120 s. In detail, the area of the transparent part of the droplet increases about 9.6 times from 90 to 120s, indicating the quick formation of the liquid.

3 Anti-freezing property.

The anti-freezing property is revealed by a side-view snapshot of the deposited water droplets on different surfaces, in which the testing method simulates a nearly real condition (Materials and Methods, Figure 3a-c and S7a). The droplet freezing time is used to quantify the anti-freezing property, which is defined as the interval between the time when water droplets are deposited on surfaces and the time when the ice forms. Figure 3d shows the freezing time of droplets on the EH surface prepared from 20 wt. % NaCl solution in comparison with those on PVA hydrogel and glass surfaces at various temperatures. At -5 and -10 °C, in contrast to the glass and PVA hydrogel surfaces with less than 100 s of droplet freezing time, the droplets on the EH surface have not been frozen even after 432000 s (5 days, which indicate that the freezing time exceeds the vertical scale in Figure 3d). The durable anti-freezing property of the EH surface is ascribed to that the ions can diffuse to the droplet, as discussed above and reported in Figure 2 and S6. The droplet freezing time on the EH surface decreases to less than 40 s due to frozen of EH prepared from 20 wt. % salted water at -20 °C (Figure 1f). Moreover, an ideal model is presented to estimate how the ice influences

electrolyte concentration of EH. The ice on EH surface is assumed to become .liquid, and the ions in EH diffuse to water (ice) and reach the equilibrium state, where the concentration of ions was roughly estimated by the mass ratio of electrolyte (Figure S7b). The small amount of ice (e.g. single droplet 5 μL) has a negligible influence on the ions concentration of the EH sample. In summary, the current EH surface makes it possible to durably prevent droplets from freezing, significantly outperforming the state-of-the-art anti-icing materials with limited freezing delay time.[4, 21, 38-39]

4 Anti-frost property.

The frost delay time of the EH surface is revealed by in situ observation of the surfaces at target relative humidity (RH) and temperature, compared with the surfaces of PVA hydrogel and glass (Figure 4a-c). The glass and EH are transparent (insets in Figure 4a (1) and (3), in which the blurry patterns are from the cooling stage) at 0s, but the PVA hydrogel freezes and show an opaque property (inset in Figure 4a (2): 0 s, Figure S8). When the moisture flux is injected, water droplets condensate and then freeze on the glass surface, where the area ratio of ice on the surface increases to 95% within 60 s. The PVA hydrogel freezes at -10 °C with opaque property, covered with the 100% area ratio of ice since 0 s (Figure 4a (2)). The EH shows a transparent property (insets in Figure 4a (3) and Video S1) and the surface does not change from 0 to 1800 s (0% area of ice), demonstrating anti-frost property within minute-scale. Furthermore, how the variable temperature and humidity influence the EH surface are revealed in Figure 4b and c, respectively. The micrographs are recorded after the samples are stored for 30 min at different temperatures (-25 - -10 °C) with the RH of 50%, or different RH (0 - 80%) at -15 °C, respectively. As shown in Figure 4b, the surface of EH has no ice after moisture flux (RH of 50%) is injected for 30 min above -15 °C; whereas the surface freezes when the temperature further decreases to -25 °C. In Figure 4c, when the RH is less than 50%, no water droplets condensate on EH surface after 30 min; when the RH increases to 80%, water gradually condensates and droplets form on the EH surface. Hence, the anti-frost function of the current EH works at temperatures down to -15 °C, despite water condensation at RH of 80%. Moreover, despite the limited time (30 min) for the anti-frost test, it is predictable that the EH could durably prevent frost formation, due to the destruction of ice via ions (Figure 2).

5 Ice adhesion strength and deicing time of EH surface.

The ice adhesion strength is a key factor to determine how easily the ice can be removed from a surface. The normal and shear ice adhesion strength of EH prepared from 20 wt. %

NaCl solution are measured at variable temperature, respectively (Figure S9). Notably, when we tested the ice adhesion at -20 °C, the EH separated from the cooling stage with the ice still attached to the EH surface, due to the larger interfacial adhesion between ice and EH than that between the stage and EH. Hence, the practical normal and shear ice adhesion of the EH surface at -20 °C are larger than 110 and 138 kPa, respectively (dotted ellipse in Figure 5a). At -15 to -5 °C, the normal and shear ice adhesion are all negligible due to the instrument capacity, where the normal and shear ice adhesion are all recorded as 0 (Figure 5a, the detail is shown in the experimental part), which is ascribed to the self-generation of sufficient lubricating layer between the interface of ice and EH (Figure 2). It is worth noting that the ice cylinder self-moves from the EH surface quickly at -15 – -5 °C during the shear ice adhesion test, showing the self-deicing property. In fact, during the ice adhesion test, the interface changes from EH-ice contact to that the lubricating layer insulates ice and EH, where the ice adhesion is influenced by the lubricating layer. With ions diffusion at interface, the thickness of the lubricating layer increases, the ice adhesion will be determined by the properties of lubricating layer finally. Furthermore, the thickness of the lubricating layer is estimated. The moving ice is hydroplaning on lubricating surface.[40] The system may change to hydrodynamic friction when ice moves. The thickness of the lubricating layer may be in the micrometer-scale when ice starts moving if the lubricating layer is roughly considered as pure water.[41] Furthermore, the concept of anti-icing temperature window is introduced to describe the effective anti-icing temperature range of EH. The critical temperature of anti-icing temperature window is defined by the EH melting point obtained from the DSC test, as the EH will freeze and the ions diffusion process is inhibited below the melting point. Hence the melting point is used as the critical temperature. Hence, the anti-icing temperature window of EH prepared from 20 wt. % NaCl solution is above ca. -17.6 °C. Moreover, the anti-icing temperature window of the EH can be controlled by infusing different types of ions with different concentrations, as shown in Figure 5b. The EHs are prepared from different concentrations and types of salted water (typical deicing agent, 20 wt. % KCl, 20 wt. % NaCl, 23.0 wt. % and 30% $CaCl_2$ solution). The DSC tests show the critical temperature of EHs can be tuned down to -48.4 °C.

The speed for self-removal of ice is quantified by the deicing time, which is defined as the interval between the time when the stage reaches the target temperature and the time when the ice starts moving. As shown in Figure S10, the ice is firstly frozen on EH surface at -25 °C (below the anti-icing temperature window), and then the EH with ice is rotated to target angle θ. Finally, the temperature of EH surface is regulated to a target temperature (within the anti-

icing temperature window). Once generation of enough lubricating layer with time, the component of gravity ($mg\sin\theta$, in which m is the mass of the ice and g is the acceleration of gravity) drives the ice to slide off the EH surface. Figure 5c shows the deicing time firstly decreases and then holds steady with the increase of θ at the temperature range of -15 to -8 °C by using the ice (5 μg). The reduction of deicing time is due to the increase of the $mg\sin\theta$ along the ice sliding direction and decrease of the normal pressure by $mg\cos\theta$. After the tilted angle of EH surface increases sufficiently, the speed for the formation of the lubricating layer dominates the deicing time, resulting in a steady deicing time.

The deicing times at -5 °C and at -8 °C (at a tilted angle beyond 20°) are recorded as 0 s, as the ice starts moving before the surface reaches the target temperature. In addition, the deicing time decreases with the increase of temperature from -15 to -5 °C at the same tilted angle, due to the faster generation of the lubricating layer at higher temperatures. Furthermore, Figure 5d reveals how the mass of ice influences the deicing time, in which the ice cylinder with the same basal area (15 mm diameter) but with variable mass (0.5-3.0 g) are used for the experiments. The deicing time firstly increases with the increase of the mass of ice, followed by a decrease. This may result from the increase of the component of gravity (via ice) and the decrease of normal pressure by $mg\cos\theta$. Figure 5e further shows the side-view optical images of ice cylinder (1.0 g) moving on the EH surface at different elapsed times as a typical example, indicating self-removal of ice (self-deicing property), which is also shown in Video S2. The ice moves from the surface can be considered as the solid-solid friction.[42] The thickness of interfacial lubricant continuously increases as the deicing time increases, resulting in the lateral threshold force at interface decreases with time. When the thickness of lubricating layer reaches the critical value, ice starts moving as $mg\sin\theta$ exceeds the lateral threshold force. Herein, the adhesion strength to ice can be roughly estimated as $mg\sin\theta$/S, where S is the contacting area between ice and EH, θ is the titled angle of the surface. For example, the adhesion strength is ca. 27.7 Pa for the system in Figure 5e. Once the ice moves, the adhesion strength for ice decreases to ca. 7.1 Pa (Figure S11), in which the difference in adhesion strength is due to the transition from static to kinetic friction.[42] In short, the order of magnitude of the deicing time is within ca. 100 s above -15 °C with the tilted angle of larger than 15° and the ice adhesion is ultralow.

6 Sustainability

The durability of the material is an important aspect of practical anti-icing applications. The lubricating layer with ions could be depleted from the EH during the deicing process, resulting in reduction of ions in the EH and thus a decrease in the anti-icing ability. Herein, as shown in the side-view schematic of the EH (Figure 6a), we propose the methods (1) and (2) for the replenishment of salted water to solve the depletion problem, based on self-diffusion of ions and water into the EH. In detail, method (1) represents the replenishment of salted water on the surface via coating method, and (2) represents the real-time replenishment of ions solution by directly connecting the EH with salted water, where the deicing time is obtained on the EH surface at -10 ^{o}C and tilted angle of 30^{o} by a mass of 1.0 g ice. The method (1) is demonstrated by coating the surface of EH with salted water. As shown in Figure 6b, the deicing time of EH with replenishment is about 10 s and keeps stable during 10 deicing cycles, indicating effective replenishment of salted water by method (1). By contrast, the deicing time of EH without replenishment increases from 10 to 130 s after 10 cycles. The deterioration of the deicing time approximately keeps stable within 6 cycles, owing to the depletion of the electrolyte to the ice. After 6 cycles, the deterioration of the deicing time decreases greatly, which may be due to the diffusion of ions inner the EH to surface. Moreover, the durability of the control sample (glass coated with 20 wt. % NaCl solution) is shown for comparison, in which the glass surface is covered with uncontinuous salted solution pattern. During the first deicing test on the position with salt, the ice slides from the control sample within 5 s, showing an ultralow ice adhesion. However, the ice freezes and does not slide during the second deicing cycle, due to the depletion of salt. The replenishment of the salted water is further demonstrated by the method (2) connecting the EH with the salted water. As the ions and water can self-diffuse in the EH, the side edge of EH (1.5×0.2 cm^2) directly contacts with the salted water to demonstrate the sustainable diffuse of ions to EH. The normalized weight of the EH samples (size: 4×1.5×0.2 cm^2) with and without the replenishment as a function of time is shown in Figure 6c. In contrast to about 50% weight loss of the EH without replenishment due to the evaporation, the weight of EH with replenishment (2) almost does not change, demonstrating the self-diffusion of salted water and the replenishment of ions from any part of EH.

Furthermore, the recovery ability of the EH is demonstrated in Figure 6d. We imitate the depletion of ions and water inside the EH by infusing the EH in water for 2 min and thereafter removing water by heat treatment. Then the EH was replenished by soaking it in the 20 wt. % NaCl solution for 2 min. After the first cycle, the normalized weight of the EH after

replenishment decreases by about 30%, which may be due to the collapse of EH during the first dry treatment. Notably, the recovery of the EH keeps stable with similar normalized weight from 2th to 10th cycle, showing the sustainable recovery property of EH. To further investigate the recovery ability, the EH is soaked in the solution for 12 h, and the normalized weight shows no obvious change. This indicates that the salted water has high mobility in EH, showing a fast recoverable property. In practical application, such fast recoverable property could potentially be used as an ice protection system for offshore platforms and marine ships, where the replenishment via seawater (typical salted water) after concentration is low cost and straight forward.

Conclusion

In this work, we have developed the sustainable and transparent anti-icing EH surfaces based on the salted water infused polymer network. According to the MD simulations and experimental results, when water droplets/ice contact the cooled EH surface, the ions inside the EH diffuse to the interface, preventing ice nucleation and destroying the ice crystals into liquid water at the interface between EH and ice/water. It has been found that the EHs have durable anti-freezing/frost properties and ultralow ice adhesion within a tunable anti-icing temperature window (down to -48.4 ^{o}C). Moreover, the ice can self-remove from EH surface within as low as 10 s at -10 ^{o}C, showing fast self-removal of ice. In addition, the EH can be quickly replenished with the salted water (e.g. seawater) by coating or directly contacting methods, resulting in sustainable anti-icing property. Our current anti-icing strategy opens up a new and low-cost strategy to prevent ice formation and accretion for multiple icing scenarios.

Supporting Information

The Supporting Information is available free of charge on the ACS Publications website.

Materials and methods, molecular dynamics simulations details, transmittance spectrum of EH, SEM and EDS results, composition of EH, schematic of the configuration of water and NaCl aqueous solution, side-view snapshot of deposited water droplets on different surfaces, digital images of PVA hydrogel and EH, schematic of normal and shear ice adhesion tests, schematic of deicing process, the displacement of ice as a function of time squared, the video of anti-frost test on EH surface, the video of ice cylinder moving with time on EH surface.

Acknowledgments

We thank Sigrid Rønneberg for the discussion. The Research Council of Norway is acknowledged for the support to the PETROMAKS2 Project Durable Arctic Icephobic Materials (project no. 255507) and for the support to the Norwegian Micro- and Nano-Fabrication Facility, NorFab (project no. 245963).

References

(1) Kreder, M. J.; Alvarenga, J.; Kim, P.; Aizenberg, J. Design of Anti-icing Surfaces: Smooth, Textured or Slippery? *Nature Reviews Materials* **2016,** *1* (1), 15003.

(2) Golovin, K.; Dhyani, A.; Thouless, M. D.; Tuteja, A. Low-interfacial Toughness Materials for Effective Large-scale Deicing. *Science* **2019,** *364* (6438), 371-375.

(3) Shen, Y. Z.; Wu, X. H.; Tao, J.; Zhu, C. L.; Lai, Y. K.; Chen, Z. Icephobic Materials: Fundamentals, Performance Evaluation, and Applications. *Progress in Materials Science* **2019,** *103*, 509-557.

(4) Chatterjee, R.; Beysens, D.; Anand, S. Delaying Ice and Frost Formation Using Phase-Switching Liquids. *Advanced Materials* **2019,** *31* (17), 1807812.

(5) Liu, J.; Zhu, C. Q.; Liu, K.; Jiang, Y.; Song, Y. L.; Francisco, J. S.; Zeng, X. C.; Wang, J. J. Distinct Ice Patterns on Solid Surfaces with Various Wettabilities. *Proceedings of the National Academy of Sciences* **2017,** *114* (43), 11285-11290.

(6) Li, Q.; Guo, Z. G. Fundamentals of Icing and Common Strategies for Designing Biomimetic Anti-icing Surfaces. *Journal of Materials Chemistry A* **2018,** *6* (28), 13549-13581.

(7) Golovin, K.; Kobaku, S. P.; Lee, D. H.; DiLoreto, E. T.; Mabry, J. M.; Tuteja, A. Designing Durable Icephobic Surfaces. *Science Advances* **2016,** *2* (3), e1501496.

(8) Li, T.; Zhuo, Y.; Håkonsen, V.; He, J.; Zhang, Z. Durable Low Ice Adhesion Foams Modulated by Submicrometer Pores. *Industrial & Engineering Chemistry Research* **2019,** *58* (38), 17776-17783.

(9) Shen, Y. Z.; Wang, G. Y.; Tao, J.; Zhu, C. L.; Liu, S. Y.; Jin, M. M.; Xie, Y. H.; Chen, Z. Anti-Icing Performance of Superhydrophobic Texture Surfaces Depending on Reference Environments. *Advanced Materials Interfaces* **2017,** *4* (22), 1807812.

(10) Khedir, K. R.; Kannarpady, G. K.; Ryerson, C.; Biris, A. S. An Outlook on Tunable Superhydrophobic Nanostructural Surfaces and their Possible Impact on Ice Mitigation. *Progress in Organic Coatings* **2017,** *112*, 304-318.

(11) Golovin, K.; Tuteja, A. A Predictive Framework for the Design and Fabrication of Icephobic Polymers. *Science Advances* **2017,** *3* (9), e1701617.

(12) He, Z.; Xiao, S.; Gao, H.; He, J.; Zhang, Z. Multiscale Crack Initiator Promoted Super-low Ice Adhesion Surfaces. *Soft Matter* **2017,** *13* (37), 6562-6568.

(13) Irajizad, P.; Al-Bayati, A.; Eslami, B.; Shafquat, T.; Nazari, M.; Jafari, P.; Kashyap, V.; Masoudi, A.; Araya, D.; Ghasemi, H. Stress-localized Durable Icephobic Surfaces. *Materials Horizons* **2019,** *6* (4), 758-766.

(14) Dou, R.; Chen, J.; Zhang, Y.; Wang, X.; Cui, D.; Song, Y.; Jiang, L.; Wang, J. Anti-icing Coating with an Aqueous Lubricating Layer. *ACS Appl Mater Interfaces* **2014,** *6* (10), 6998-7003.

(15) Yaling, W.; Xi, Y.; Shuwang, W.; Qunyang, L.; Jianyong, L.; Jianjun, W.; Lei, J. Bioinspired Solid Organogel Materials with a Regenerable Sacrificial Alkane Surface Layer. *Advanced Materials* **2017,** *29* (26), 1700865.

(16) Kim, P.; Wong, T. S.; Alvarenga, J.; Kreder, M. J.; Adorno-Martinez, W. E.; Aizenberg, J. Liquid-infused Nanostructured Surfaces with Extreme Anti-ice and Anti-frost Performance. *ACS Nano* **2012,** *6* (8), 6569-6577.

(17) Lv, J.; Yao, X.; Zheng, Y.; Wang, J.; Jiang, L. Antiadhesion Organogel Materials: From Liquid to Solid. *Adv Mater* **2017,** *29* (45), 1703032.

(18) He, Z.; Wu, C.; Hua, M.; Wu, S.; Wu, D.; Zhu, X.; Wang, J.; He, X. Bioinspired Multifunctional Anti-icing Hydrogel. *Matter* **2020,** *2* (3), 723-734.

(19) Chen, J.; Dou, R. M.; Cui, D. P.; Zhang, Q. L.; Zhang, Y. F.; Xu, F. J.; Zhou, X.; Wang, J. J.; Song, Y. L.; Jiang, L. Robust Prototypical Anti-icing Coatings with a Self-lubricating Liquid Water Layer between Ice and Substrate. *ACS Applied Materials & Interfaces* **2013,** *5* (10), 4026-4030.

(20) Kondo, H.; Hanada, Y.; Sugimoto, H.; Hoshino, T.; Garnham, C. P.; Davies, P. L.; Tsuda, S. Ice-binding Site of Snow Mold Fungus Antifreeze Protein Deviates from Structural Regularity and High Conservation. *Proceedings of the National Academy of Sciences* **2012,** *109* (24), 9360-9365.

(21) He, Z.; Xie, W. J.; Liu, Z.; Liu, G.; Wang, Z.; Gao, Y. Q.; Wang, J. Tuning Ice Nucleation with Counterions on Polyelectrolyte Brush Surfaces. *Science Advances* **2016,** *2* (6), e1600345.

(22) Liu, F.; Wang, Z.; Pan, Q. Intelligent Icephobic Surface toward Self-Deicing Capability. *ACS Sustainable Chemistry & Engineering* **2019,** *8* (2), 792-799.

(23) Varanasi, K. K.; Deng, T.; Smith, J. D.; Hsu, M.; Bhate, N. Frost formation and ice adhesion on superhydrophobic surfaces. *Applied Physics Letters* **2010,** *97* (23), 234102.

(24) Chen, J.; Liu, J.; He, M.; Li, K.; Cui, D.; Zhang, Q.; Zeng, X.; Zhang, Y.; Wang, J.; Song, Y. Superhydrophobic Surfaces Cannot Reduce Ice adhesion. *Applied Physics Letters* **2012,** *101* (11), 111603.

(25) He, Z.; Zhuo, Y.; He, J.; Zhang, Z. Design and Preparation of Sandwich-like Polydimethylsiloxane (PDMS) Sponges with Super-low Ice Adhesion. *Soft Matter* **2018,** *14* (23), 4846-4851.

(26) He, Z.; Zhuo, Y.; Wang, F.; He, J.; Zhang, Z. Understanding the Role of Hollow Sub-surface Structures in Reducing Ice Adhesion Strength. *Soft Matter* **2019,** *15* (13), 2905-2910.

(27) Li, T.; Zhuo, Y.; Håkonsen, V.; Rønneberg, S.; He, J.; Zhang, Z. Epidermal Gland Inspired Self-Repairing Slippery Lubricant-Infused Porous Coatings with Durable Low Ice Adhesion. *Coatings* **2019,** *9* (10), 602.

(28) Koshio, K.; Waku, T.; Hagiwara, Y. Ice-phobic Glass-substrate Surfaces Coated with Polypeptides Inspired by Antifreeze Protein. *International Journal of Refrigeration* **2020,** *114*, 201-209.

(29) Yamazaki, T.; Tenjimbayashi, M.; Manabe, K.; Moriya, T.; Nakamura, H.; Nakamura, T.; Matsubayashi, T.; Tsuge, Y.; Shiratori, S. Antifreeze Liquid-Infused Surface with High Transparency, Low Ice Adhesion Strength, and Antifrosting Properties Fabricated through a Spray Layer-by-Layer Method. *Industrial & Engineering Chemistry Research* **2019,** *58* (6), 2225-2234.

(30) Niemelä-Anttonen, H.; Koivuluoto, H.; Tuominen, M.; Teisala, H.; Juuti, P.; Haapanen, J.; Harra, J.; Stenroos, C.; Lahti, J.; Kuusipalo, J.; Mäkelä, J. M.; Vuoristo, P. Icephobicity of Slippery Liquid Infused Porous Surfaces under Multiple Freeze-Thaw and Ice Accretion-Detachment Cycles. *Advanced Materials Interfaces* **2018,** *5* (20), 1800828.

(31) Liu, Z.; He, Z.; Lv, J.; Jin, Y.; Wu, S.; Liu, G.; Zhou, F.; Wang, J. Ion-specific Ice Propagation Behavior on Polyelectrolyte Brush Surfaces. *RSC Advances* **2017,** *7* (2), 840-844.

(32) Guo, Q.; He, Z.; Jin, Y.; Zhang, S.; Wu, S.; Bai, G.; Xue, H.; Liu, Z.; Jin, S.; Zhao, L.; Wang, J. Tuning Ice Nucleation and Propagation with Counterions on Multilayer Hydrogels. *Langmuir* **2018,** *34* (40), 11986-11991.

(33) Wang, F.; Xiao, S.; Zhuo, Y.; Ding, W.; He, J.; Zhang, Z. Liquid Layer Generators for Excellent Icephobicity at Extremely Low Temperatures. *Materials Horizons* **2019,** *6* (10), 2063-2072.

(34) Quintero, S. M. M.; Ponce F, R. V.; Cremona, M.; Triques, A. L. C.; d'Almeida, A. R.; Braga, A. M. B. Swelling and Morphological Properties of Poly(vinyl alcohol) (PVA) and

Poly(acrylic acid) (PAA) Hydrogels in Solution with High Salt Concentration. *Polymer* **2010,** *51* (4), 953-958.

(35) Sun, Q. Raman Spectroscopic Study of the Effects of Dissolved NaCl on Water Structure. *Vibrational Spectroscopy* **2012,** *62*, 110-114.

(36) Koop, T.; Luo, B.; Tsias, A.; Peter, T. Water Activity as the Determinant for Homogeneous Ice Nucleation in Aqueous Solutions. *Nature* **2000,** *406* (6796), 611-614.

(37) Sui, X.; Guo, H.; Chen, P.; Zhu, Y.; Wen, C.; Gao, Y.; Yang, J.; Zhang, X.; Zhang, L. Zwitterionic Osmolyte-Based Hydrogels with Antifreezing Property, High Conductivity, and Stable Flexibility at Subzero Temperature. *Advanced Functional Materials* **2019,** *30* (7), 1907986.

(38) Aydin, D.; Akolpoglu, M. B.; Kizilel, R.; Kizilel, S. Anti-icing Properties on Surfaces through a Functional Composite: Effect of Ionic Salts. *Acs Omega* **2018,** *3* (7), 7934-7943.

(39) Akhtar, N.; Anemone, G.; Farias, D.; Holst, B. Fluorinated Graphene Provides Long Lasting Ice Inhibition in High Humidity. *Carbon* **2019,** *141*, 451-456.

(40) Daniel, D.; Timonen, J. V. I.; Li, R.; Velling, S. J.; Aizenberg, J. Oleoplaning Droplets on Lubricated Surfaces. *Nature Physics* **2017,** *13* (10), 1020-1025.

(41) Kietzig, A.-M.; Hatzikiriakos, S. G.; Englezos, P. Physics of Ice Friction. *Journal of Applied Physics* **2010,** *107* (8), 081101.

(42) Gao, N.; Geyer, F.; Pilat, D. W.; Wooh, S.; Vollmer, D.; Butt, H.-J.; Berger, R. How Drops Start Sliding Over Solid Surfaces. *Nature Physics* **2018,** *14* (2), 191-196.

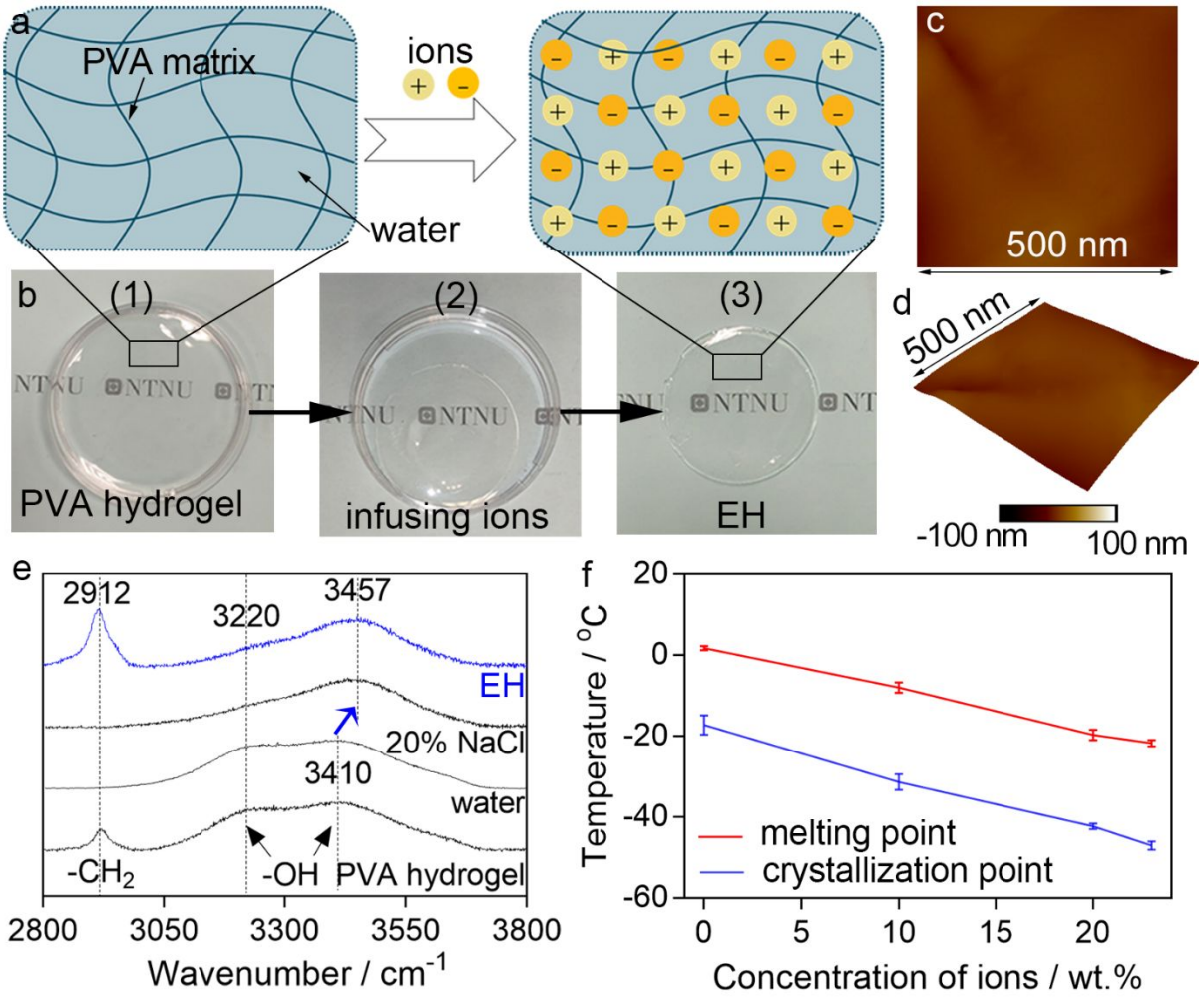

Figure 1 Fabrication and properties of electrolyte hydrogel (EH) prepared from 20 wt. % NaCl solution. (a) Schematic and (b) experimental process of fabricating EH. (c) Two- and (d) three-dimensional AFM images of EH surface. (e) Raman spectra of EH in comparison with 20 wt. % NaCl aqueous solution, water and PVA hydrogel. (f) The relationship between concentration of ions and corresponding crystallization/melting point of EH.

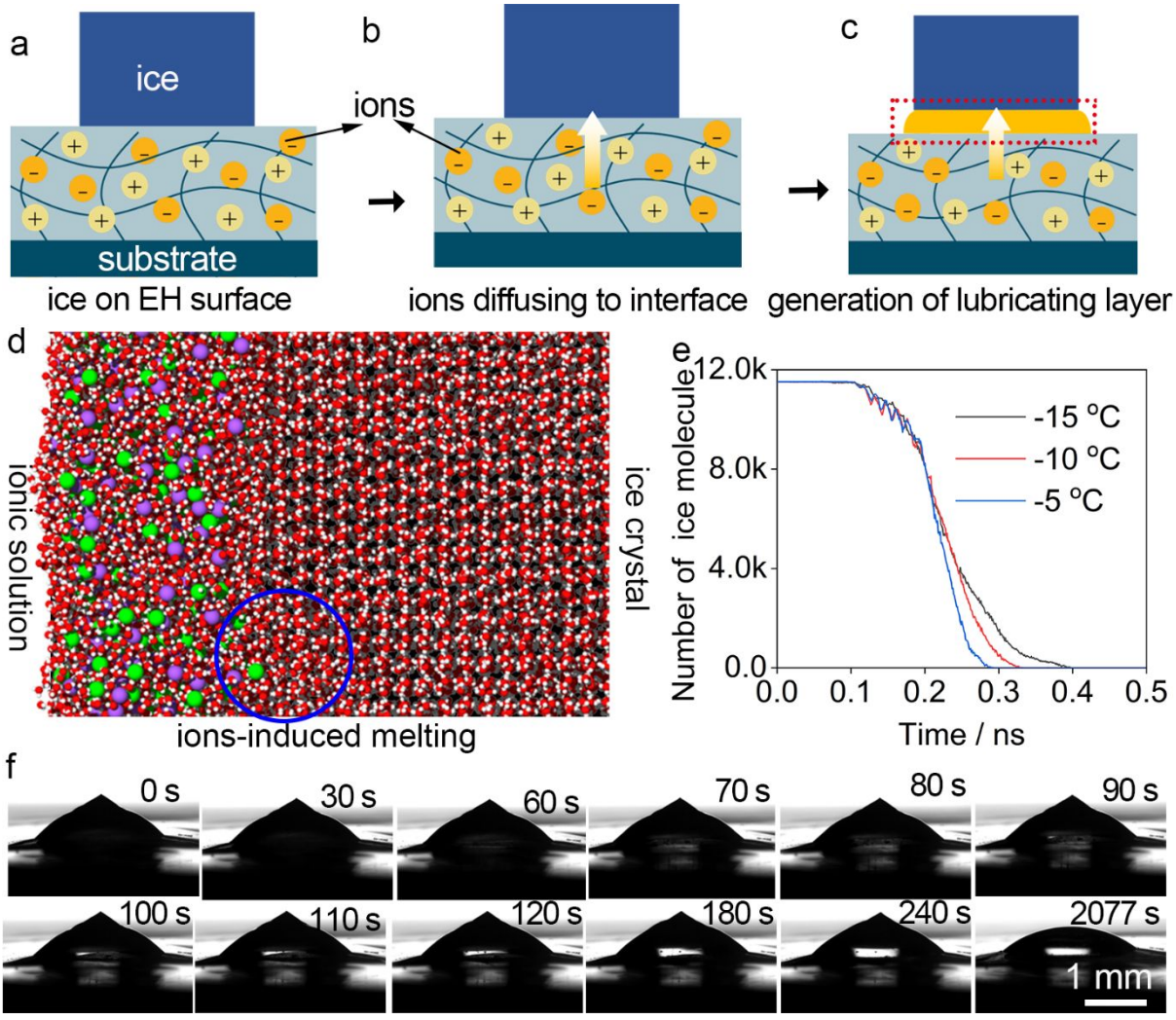

Figure 2 Self-generation of lubricating layer on EH surface. (a-c) Schematic of the generation of lubricating layer. (d) An MD intermediate state image of interaction between ice and ions at -10 °C. (e) Number of ice molecules as a function of time at variable temperature by MD simulation. (f) The melting process of ice on EH surface prepared from 20 wt. % NaCl solution at -10 °C.

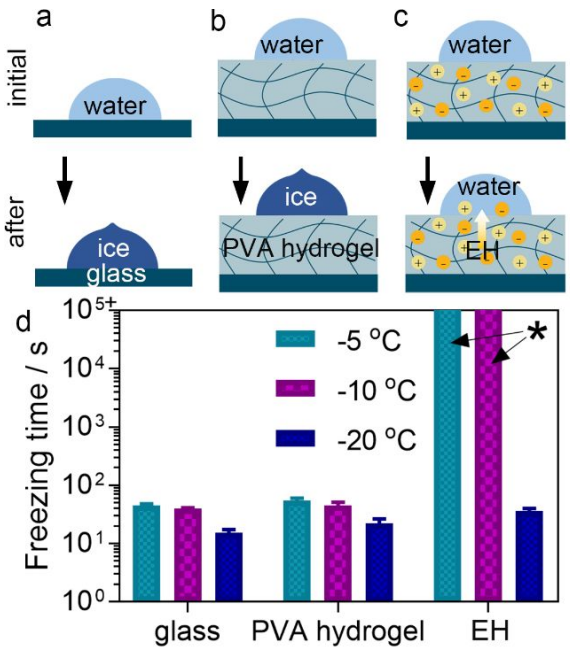

Figure 3 Anti-freezing properties of EH surface prepared from 20 wt. % NaCl solution. (a-c) Schematic of droplets freezing process on different surfaces at -10 °C. (d) Freezing time of water droplets on EH surface in comparison with PVA hydrogel and glass surfaces at different temperature. The asterisk (*) in (d) indicates that the water droplets have not been frozen at -5 and -10 °C after 43200 s.

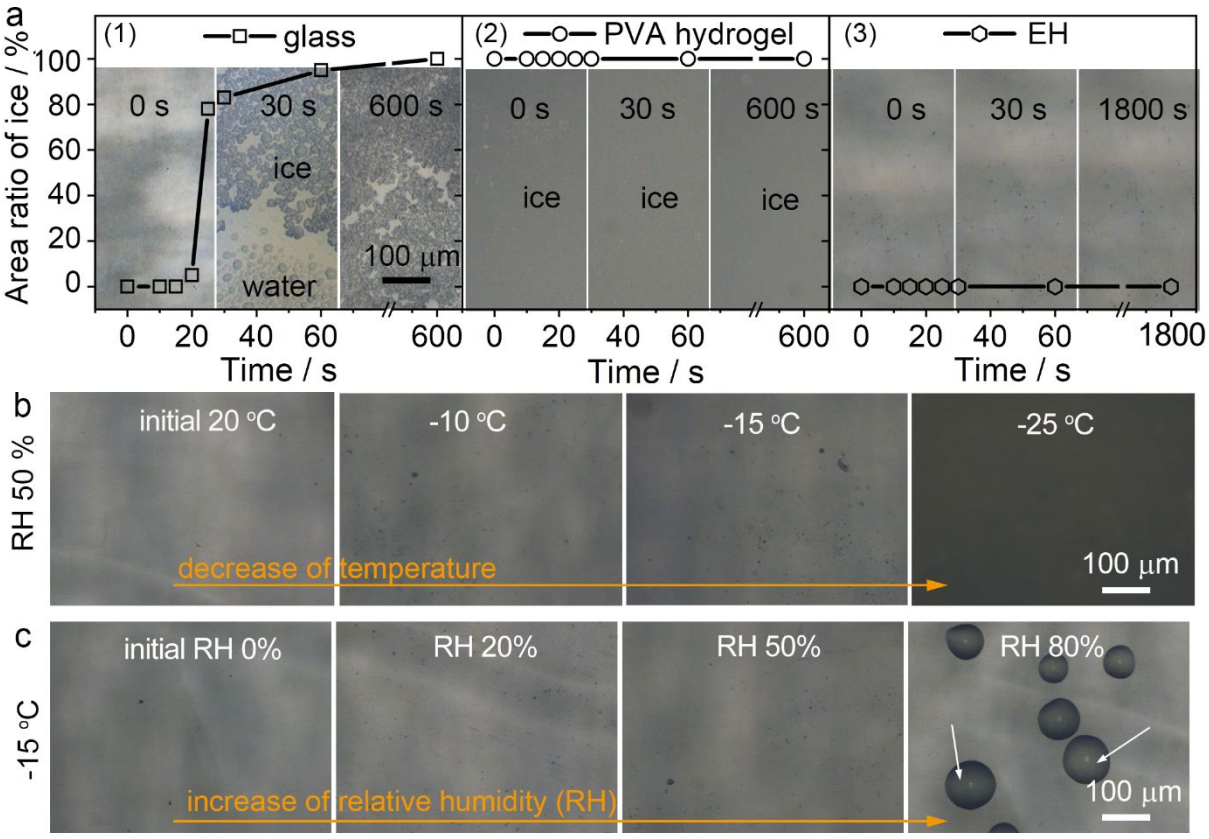

Figure 4 Anti-frost property of EH surface prepared from 20 wt. % NaCl solution. (a) Area ratio of formed ice on different surfaces as a function of time at -10 °C and 50% RH. The insets in (a) are micrographs of surfaces at different elapsed times. (b) Micrographs of EH surfaces with decrease of temperature after being stored at RH of 50% for 30 min. (c) Micrographs of EH surfaces with increase of humidity after storage at -15 °C for 30 min. The white arrows in (c) indicate the condensed liquid water droplets on EH surface.

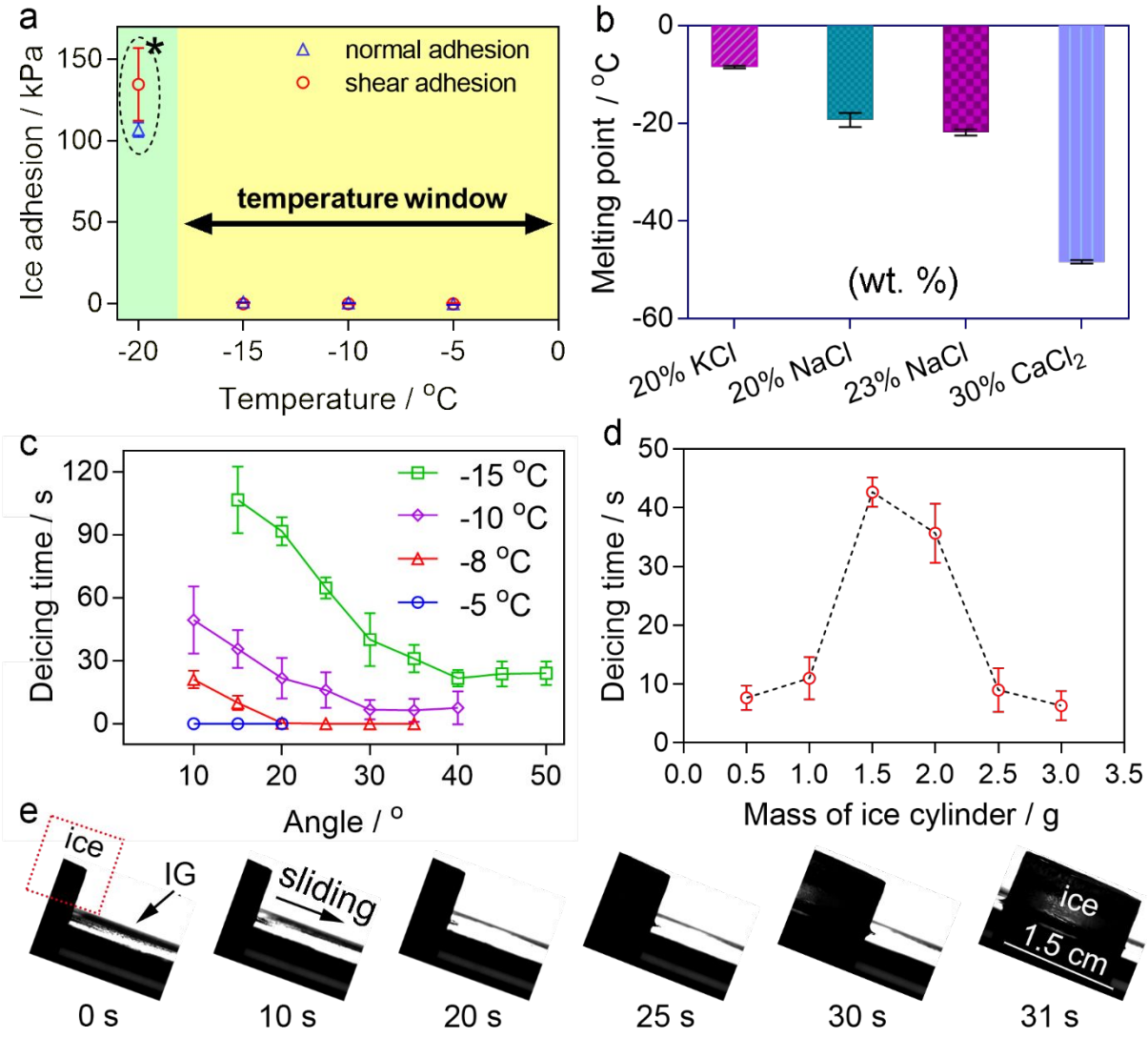

Figure 5 Ice adhesion strength and deicing time of EH surfaces. (a) Normal and shear ice adhesion of EH surfaces prepared from 20 wt. % NaCl solution with variable temperatures. The asterisk in (a) represents the adhesion between the cooling stage and EH, as the ice adhesion of EH at -20 °C is higher than the adhesion between the stage and the EH. The temperature window in (a) represents the anti-icing temperature range, where the ice adhesion is ca. 0 Pa. (b) EHs with controlled anti-icing temperature window by infusing different kinds of ions sources with different concentrations. The deicing time of EH surfaces with different (c) tilted angles and (d) mass of ice cylinder with the same circular basal area (15 mm diameter) at -10 °C and the tilted angle of 30°. (e) Images of ice cylinder (1.0 g) moving on the EH surface with time at -10 °C and a tilted angle of 30°.

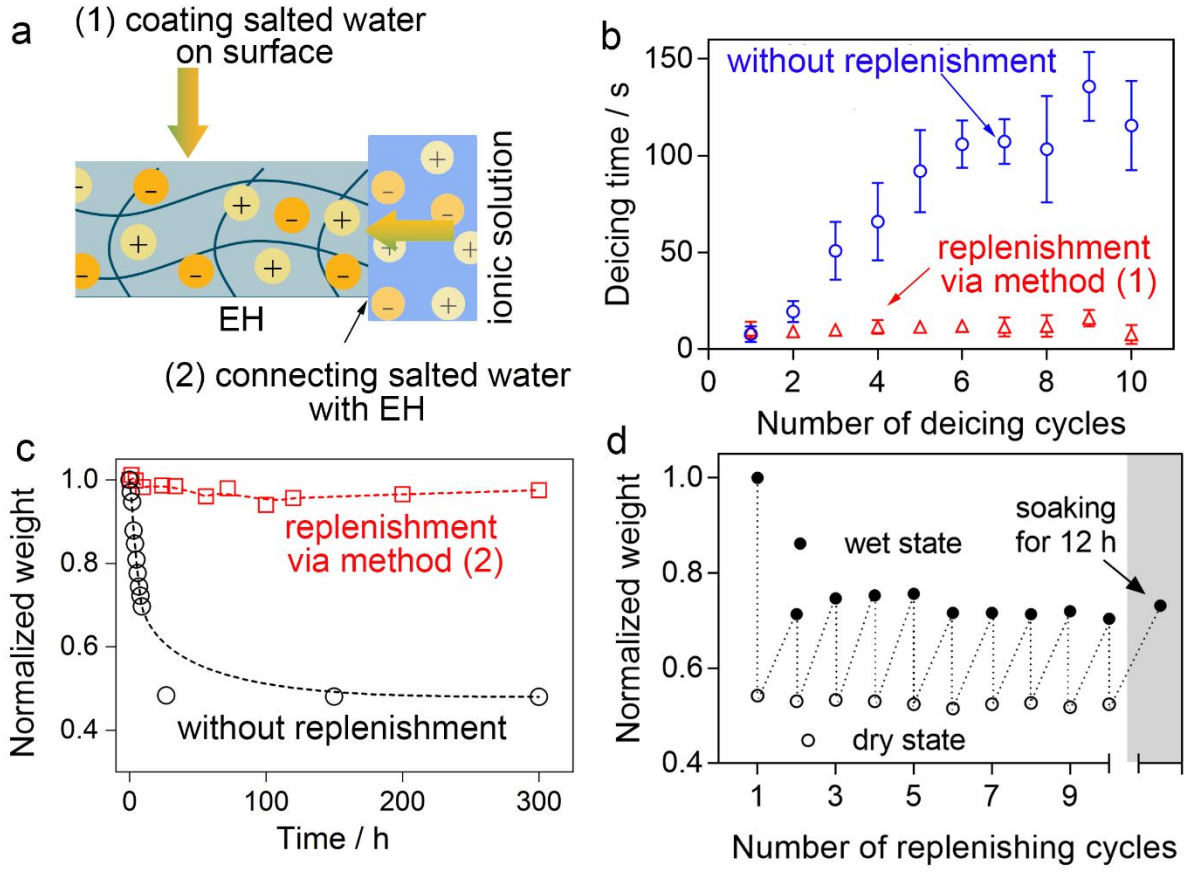

Figure 6 Replenishment of salted water into EH prepared from 20 wt. % NaCl solution. (a) Schematic of two strategies for replenishment. In detail, (1) represents the replenishment of salted water on the surface via coating method, and (2) represents the replenishment of ions solution by real-timely connecting the EH with salted water. (b) The deicing time of EH with and without replenishment via method (1) as a function of deicing cycles. (c) Normalized weight of EH with and without replenishment via method (2). (d) Normalized weight of EH during replenishing cyclic tests and after soaking of the EH for 12h (grey part).

TOC